Excited State Dynamics of 6-Thioguanine

Faady M. Siouri, Samuel Boldissar, Jacob A. Berenbeim, Mattanjah S. de Vries*

Department of Chemistry and Biochemistry, University of California, Santa Barbara, CA 93016-9510

Abstract

Here we present the excited state dynamics of jet-cooled 6-thioguanine (6-TG), using resonance-enhanced multiphoton ionization (REMPI), IR-UV double resonance spectroscopy, and pump-probe spectroscopy in the nanosecond and picosecond time domains. We report data on 2 thiol tautomers, which appear to have different excited state dynamics. These decay to a dark state, possibly a triplet state, with rates depending on tautomer form and on excitation wavelength, with the fastest rate on the order of 10^{10} s^{-1}. We also compare 6-TG with 9-enolguanine, for which we observed decay to a dark state with a two orders of magnitude smaller rate. At increased excitation energy (~ +500 cm^{-1}) an additional pathway appears for the predominant thiol tautomer. Moreover, the excited state dynamics for 6-TG thiols is different from that recently predicted for thiones.

1. Introduction

The DNA and RNA bases have a built-in protection mechanism against UV radiative damage. When they absorb UV light, they return safely to the electronic ground state in less than a picosecond by internal conversion (IC). This ultrafast IC dominates alternative relaxation pathways, such as intersystem crossing (ISC), so potentially harmful photochemical processes are largely averted. The availability of rapid IC pathways depends critically on molecular structure. This dependence results from the fact that the conical intersections that mediate IC occur at molecular geometries that differ strongly from ground state minimum geometries. Therefore the excited state dynamics of nucleobases can differ drastically for different derivatives,[1-9] analogues,[10-12] and even tautomers.[13-15] Many derivatives and analogues of the canonical nucleobases that could serve as alternative bases lack the UV protection afforded by rapid internal conversion. This difference suggests a possible prebiotic photochemical selection of nucleobases on an early earth. In the case of guanine (G), the keto tautomer, which is prevalent in DNA, is characterized by rapid IC in contrast to enol and imino tautomers.[15-24] When the oxygen atom in DNA is replaced with a sulfur atom, the photochemistry changes dramatically due to the heavy atom effect on spin-forbidden transitions.[25] Canonical DNA bases absorb UVB (290-320 nm); whereas, sulfur substituted DNA analogues such as 6-thioguanine (6-TG), absorb UVA (320-400 nm).[12, 26-28] Yu et al. reported a significant increase in intersystem crossing rate for 2-thiouracil relative to uracil in the gas phase, following excitation at 295 and 260 nm, respectively[29]. The comparison of the excited state dynamics of G versus 6-TG has so-far been limited to their keto and corresponding thione tautomers.[30-31] The photoproducts and photochemistry of the enol and corresponding thiol tautomers have not been studied in great detail. In this work we find significant transition rates to a dark state, most likely a triplet state, with estimated quantum yields of the order of 25% for enol G and considerably higher rates for thiol 6-TG. Here and throughout quantum yield estimates represent an upper limit as we may not be observing all decay processes in our experiment.

6-TG and other thiopurines are effective anti-inflammatory, anticancer, and immunosuppressive drugs used for over 50 years,[32] however, prolonged treatment with 6-TG has been associated with a 65-250 times increased risk of skin cancer.[33] 6-TG is of interest because it can be incorporated into a patient's DNA,[34] increasing skin sensitivity to UVA radiation. Once 6-TG is converted into 6-TG nucleotide, it replaces the guanine in the patient's DNA.[35] Excitation of DNA-6TG with UVA radiation generates a series of reactions leading to the formation of reactive oxygen[36] species such as singlet oxygen that can damage both DNA and proteins.[37-38] Other consequences of UVA interaction with DNA 6-TG includes DNA and protein oxidation, DNA-protein cross linking, DNA strand breakage, and DNA interstrand cross linking.[39]

Guanine is known to relax to the ground state by internal conversion with lifetimes of 140 fs and 2.3 ps,[24] and by fluorescence on the timescale of 12 to 25 ns.[40] These fast relaxation times are indicative of a nucleobase that efficiently dissipates internal energy introduced through UV excitation. However, the fast decay was observed in femtosecond pump-probe experiments, performed with a 267 nm excitation pulse and 400 nm probe pulse, which do not map out the complete excited state dynamics. Furthermore, these femtosecond experiments lack tautomer

selectivity. In solution guanine is primarily in the keto form. In the gas phase, four guanine tautomers were observed in molecular beams by resonance enhanced multiphoton ionization (REMPI); two imino, and two enol forms.[18, 41] Choi et al. observed keto tautomers in helium droplets which suggests the keto tautomers are present in molecular beams but unobserved by multiphoton ionization.[42] In the present work, we evaluate the excited state lifetime of the 9-H enol guanine and compare it with that of thiol 6-TG. Research on 6-TG has focused on exploring the excited state dynamics of the thione tautomer, but no studies have been reported on the thiol tautomer.[30, 43-45] Reichardt et al. investigated the excited state dynamics of 6-thioguanosine in phosphate buffer and in acetonitrile solutions via femtosecond broadband transient absorption spectroscopy coupled with quantum chemical calculations.[43] They determined that in aqueous buffer solution, ~ 80% of the S_2 ($\pi\pi^*$) excited state population decays by ultrafast intersystem crossing to T_3 ($n\pi^*$) which is ~0.1 eV below the S_2 Franck-Condon (FC) region, suggesting a strong spin-orbit coupling between these two states. However, Martínez-Fernández et al have later argued that the proposed channel is not the correct pathway to the triplet manifold.[30, 44] Instead, they used *ab initio* calculations to show that the dominant pathway is $S_2 \rightarrow S_1 \rightarrow T_2 \rightarrow T_1$. Moreover, Martínez-Fernández et al assigned T_3 as ($\pi\pi^*$) instead of ($n\pi^*$). As a result, Martínez-Fernández et al. determined that the S_2 state ($\pi\pi^*$) and T_3 state ($\pi\pi^*$) negligibly coupled at the FC and S_2 minimum structures. Both authors however agreed that internal conversion and intersystem crossing compete in the relaxation mechanism to the ground state with the intersystem crossing pathway being the major pathway and $S_2 \rightarrow S_1 \rightarrow S_0$ being the minor pathway.

Here we present the tautomeric characterization and excited state dynamics of jet-cooled guanine in the enol form (G_e) and of 6-thioguanine (6-TG) as an alternative nucleobase and as a case study into heavy-atom effects on ISC and application of El-Sayed's rules.[46] We collected 1 and 2-color REMPI on isolated 6-TG, with IR-UV characterization, and performed nanosecond and picosecond pump-probe spectroscopy on G_e and 6-TG to construct a model of excited state decay from the origin up to ~900 cm^{-1} excess internal energy.

2. Methods

Experimental

The instrument has been previously described in detail and only a brief description of the experimental setup follows.[47] Samples (6-thioguanine, TCI 95%) are mixed with carbon black and placed on a translating graphite substrate directly in front of a pulsed molecular beam valve, based on a piezo cantilever design.[48] They are laser desorbed by a focused Nd:YAG laser (1064 nm, ~ 1 mJ/cm^2), then entrained in a supersonic molecular beam of argon (8 atm backing pressure, 15 μsec pulse width) at a repetition rate of 10 Hz. The cold, neutral molecules are ionized by REMPI and are subsequently detected in a reflectron time of flight mass spectrometer. One-color nanosecond REMPI is carried out with the frequency doubled output of a Lumonics HD-300 tunable dye laser (2 mJ/pulse, 8 ns pulse length, 0.04 cm^{-1} spectral linewidth).

The picosecond REMPI spectroscopic and pump-probe delay measurements are performed with an Ekspla PL2251 Nd:YAG laser system producing ~ 30 ps laser pulses. The 355 nm output

pumps an Ekspla PG401 tunable optical parametric generator (OPG) (UV output of 80-120 μJ/pulse, 30 ps pulse length, ~ 6 cm^{-1} spectral linewidth). 6-TG is excited by the OPG UV and ionized by 266 nm, fourth harmonic of the ps pump laser, which is mechanically delayed up to 2 ns before colineation with the OPG beam. A variable delay between OPG UV laser and an excimer laser (193 nm, 1.5-2 mJ/pulse) is used for pump-probe measurements in the nanosecond range.

For IR-UV double resonant spectroscopy a Laser Vision optical parametric oscillator/amplifier (OPA/OPA) (mid-IR output over the range 3,200-3,800 cm^{-1} of ~3-5 mJ/pulse, 3 cm^{-1} spectral linewidth) precedes the ns REMPI by 200 ns. We perform double resonant spectroscopy with two different pulse sequences in this report: in mode I we scan the IR at a fixed UV probe wavelength and in mode II we scan the UV with a fixed IR burn wavelength. In mode I the IR laser is scanned while the UV laser is fixed on one vibronic transition and signal depletes when the IR laser becomes resonant with that ground state population. The resulting ion-dip spectrum represents the ground state IR spectrum of a single tautomer, selected by the UV probe wavelength. This IR spectrum can be compared with calculated IR frequencies to determine the specific tautomer of the selected vibronic transition. In mode II the IR laser is set to a tautomer-specific vibrational resonance and we scan the UV laser, comparing spectra with IR laser on and off. The difference spectrum identifies peaks in the UV spectrum that arise from the same tautomer.

We performed pump-probe experiments on both the nanosecond and picosecond timescale to determine which types of processes are occurring in this system. By combining information from both time domains and monitoring lifetimes as a function of excitation energy, it is possible to gain an understanding of the excited state dynamics involved in deactivation.

The behavior as a function of time of each decay channel derives from the kinetic equations and from solving the system of ordinary differential equations with boundary conditions shown in equation 1, where p(t) refers to a primary pathway which is populated at zero delay time and which, with a time constant τ_n, fills a secondary pathway, s(t), which in turn decays with a time constant τ_m. Since measurements are made with a finite pulse width laser, the measured response is a convolution of the instrument response function (IRF) with each of the pump and probe pulses where the IRF is represented by a Gaussian centered around t_0.

The standard deviation of the Gaussian is fitted for each profile rather than using a single value, as reported by Lipert et al.[49] and results in FWHM values which ranged from half to full width of the experimental laser pulses. After convoluting the exponential decays, which gives the excitation profile, the profile is convoluted again with the probe pulse as performed by Spesyvtsev and shown in equations 2a-b.[50] The excitation profile, P(t), consists of a sum of all primary and secondary pathways, where the secondary pathways are multiplied by an ionization efficiency factor (ϕ_{ion}) relative to the primary pathway, as shown in equation 2a. The excitation profile is convolved with 2 Gaussians centered at different t_0 with standard deviation σ in equation 2b. This double convolution is then scaled with a factor f which accounts for the signal intensity being in arbitrary units. The data are fit using a sum of the convolutions in 2b and a Gaussian centered around maximum signal, as performed by Kang et al.[31] We performed all

fitting with the Mathematica 10 package which employed the Levenberg–Marquardt algorithm for least squares fitting.[51]

$$\frac{dp}{dt} = -\frac{1}{\tau_n}\boldsymbol{p}(t,\tau_n), \qquad \frac{ds}{dt} = \frac{1}{\tau_n}\boldsymbol{p}(t,\tau_n) - \frac{1}{\tau_m}\boldsymbol{s}(t,\tau_m) \qquad \text{eqn 1}$$

$$\boldsymbol{P}(t) = \sum_{n=1}^{N}\sum_{m=1}^{M}\boldsymbol{p}(t,\tau_n) + \boldsymbol{\phi}_{ion}\,\boldsymbol{s}(t,\tau_m) \qquad \text{eqn 2a}$$

$$\boldsymbol{I}(t) = \boldsymbol{f}\int_0^t \boldsymbol{G}\left(t-t'', t_0^{probe}, \sigma\right)\int_0^t \boldsymbol{G}\left(t-t', t_0^{pump}, \sigma\right)\boldsymbol{P}(t)\,dt'dt'' \qquad \text{eqn 2b}$$

Computational Methods

Starting structures for both thiol and thione structures were optimized using the B3LYP hybrid functional with a 6-31+G(2d,p) basis set. The shorthand notation of these structures will include a number, 7 or 9, which indicates which nitrogen is sp^3 hybridized, and a letter, e or k, which indicates whether the structure is a thiol or thione, respectively. This nomenclature was adopted to be consistent with the equivalent enol and keto designations for guanine. These structures were then further optimized using MP2/6-31+G(2d,p), which were then used to perform an anharmonic frequency analysis where ground state minima were confirmed by the absence of imaginary frequencies. The simulated spectra arise from anharmonic frequencies with harmonic intensities using a Lorentzian shape and FWHM of 1 cm^{-1}. The MP2 optimized structures were used for single point energy calculations at the CCSD and EOM-CCSD level with the same basis set. These levels of theory provide good accuracy electronic energies for the ground and electronically excited states, respectively. These computations were performed by using *Gaussian 09*.[52]

Preliminary *ab initio* molecular dynamic simulations were performed on 9e-6TG using surface hopping including arbitrary couplings (SHARC) to augment interpretation of the experimental excited state lifetimes with a first-order relaxation mechanism.[53-54] The package developed by Gonzalez and coworkers performs high accuracy *ab initio* calculations and modifies nuclear positions as a function of time to obtain molecular dynamic information. The quantum calculations within SHARC were performed with the *Molpro* interface.[55] A limited number of trajectories (10) were run which included three singlet and three triplet electronic states, so that intersystem crossing information could be obtained as well as singlet internal conversion. Once an internal conversion (IC) or intersystem crossing (ISC) geometry was found in a *SHARC* trajectory, the geometry was verified by performing a single point energy calculation with *Gaussian 09*, followed by a linear interpolation of internal coordinates (LIIC) from the Frank-Condon geometry to the intersection of interest. Both *Gaussian 09* and *Molpro* simulations employed the state averaged complete active space self-consistent field method (SA-CASSCF). The active space used in this method consisted of 10 electrons in 10 orbitals (10,10), and used the 6-31G* basis set.

It should be emphasized that the SHARC simulations and LIIC theory were done at a level different from the aforementioned electronic state static energy calculations and anharmonic frequency analysis. We chose this approach to achieve rigorous but preliminary theory at low computational cost and future work on these 6-TG and G enol systems is needed with higher

order perturbation methods, such as CASPT2, given the documented complexity of purine excited state models.[56]

3. Results

REMPI

Figure 1 shows the REMPI spectrum of jet-cooled 6-TG in the frequency range 32,330 - 33,330 cm^{-1}. The black trace shows nanosecond one-color (1C) REMPI. The spectrum exhibits a sharp red-most band at 32,343 cm^{-1}, which we assume to be a 0_0^0 band and similarly sharp vibronic bands up to +290 cm^{-1}, after which the spectral features lose intensity and congest. The red trace shows the same spectrum with picosecond excitation. In this case the signal is lower so we used two-color (2C) REMPI in which the second color consisted of 266 nm picosecond pulses. Two-color ionization with nanosecond 193 nm ionization is not shown but shows features identical to ionization at 266 nm. The excitation laser in the 2C-REMPI has a spectral linewidth of 6 cm^{-1}, as opposed to 0.04 cm^{-1} for the laser in the 1C scan. Above 500 cm^{-1} the nanosecond signal is strongly reduced in contrast to the picosecond signal. This observation points to a decrease in excited state lifetime with increasing excitation energy, corresponding to a deactivation pathway with a barrier of the order of 500 cm^{-1}.

Structural Determination

Figure 2 shows a double resonant spectrum recorded in mode I, with the UV probe laser fixed at 32,343 cm^{-1} together with calculated anharmonic IR frequencies for four different tautomers. Figure 3 shows the optimized structures of the different tautomers. The simulated spectra of both thiol structures fit the experimental spectrum, while none of the thione spectra fit, which was previously confirmed by Kasende.[57] 6-TG thiones have 2 bands in the red part of the spectrum, whereas only one band is present in the thiols (3,470 cm^{-1}), representing the $(NH_2)_{sym}$ stretch. Moreover, the thione bands do not line up with the experimental data, particularly the highest energy band, the $(NH_2)_{asym}$ stretch, which appears ~50 cm^{-1} lower than the highest frequency measured. The calculated and measured intensities are well matched with the N7H/N9H stretch band at 3,510 cm^{-1}, which is the most intense, followed by the $(NH_2)_{sym}$ stretch at 3,470 cm^{-1} and $(NH_2)_{asym}$ stretch at 3,584 cm^{-1} with nearly identical intensities but slightly more intense at 3,470 cm^{-1}. We did search for the SH stretch which is calculated to be around 2,662 cm^{-1}. However, we did not detect the peak in that region which is most likely due to a weak oscillator strength which is calculated to be less than 10% of the least intense NH/NH_2 peaks.

Vibrational analysis is typically the most direct way of determining which isomers are present in the molecular beam; however, Figure 2 shows that it is difficult to distinguish between 9e and 7e tautomers. As calculated (Figure 3**)** the 9e is ~9 kJ/mol higher in energy than the lowest energy tautomer, and the 7e is ~30 kJ/mol higher in energy than the lowest energy tautomer. Past work in our lab on the nucleobase adenine showed that only the lowest energy isomer was present, where the next lowest energy isomer was calculated to be at ~33 kJ/mol higher energy than the one observed.[58] For this reason, we tentatively assign the UV origin species as 9e. We do not rule out the possibility of 7e or perhaps a 9e-stereoisomer being present given the ambiguity of their

IR spectra. The discussion will proceed focusing on 9e, but keeping these alternatives in consideration.

So far, we have shown that 9e and possibly 7e are the tautomers present when probing at the origin. Typically, UV-UV hole-burning spectroscopy is used to determine the number of tautomers in a REMPI scan; however, the presence of a long-lived dark state, which we discuss below, interferes with this approach. For UV-UV hole-burning to work, the probe laser should only produce ions from the ground state and this signal should be reduced when the ground state is depleted resonantly by the burn laser. However, when the burn laser populates a long-lived dark state, the probe laser can still produce ions indiscriminately from that dark state even at the burn laser resonances. Since it is not practical to perform double resonant spectroscopy in mode I, scanning the IR with the UV wavelength fixed, at each successive UV peak, we performed double resonant spectroscopy in mode II.

We set the burn laser to 3,584 cm^{-1} 200 ns prior to the UV probe laser which was then scanned to record the IR-UV hole burning spectrum. We chose the $(NH_2)_{asym}$ stretch because it is a good thiol indicator (Figure 2). There is no marker frequency that can distinguish between 7e and 9e tautomers as they share very similar IR spectra. We obtained spectra with IR laser off and IR laser on, where a decrease in signal indicates shared IR resonance with the origin transition and theoretically the same isomer. The result, shown in Figure 4, indicates that the entire UV spectrum in this range correlates with the same IR marker frequency and thus exclusively with thiol tautomers.

Pump-Probe

6-Thioguanine

In the following discussion, we refer to the UV excitation peaks by their energy relative to the origin at 32,343 cm^{-1}.

Table 1 lists fitting parameters from the picosecond and nanosecond pump-probe experiments. When fitting the picosecond pump-probe traces, shown in Figure 5**,** all traces except for 47 cm^{-1} and 290 cm^{-1} are fit with a primary decay (τ_1) on the order of hundreds of picoseconds, which populates a secondary state. The lifetime of the secondary state (τ_2) can only be determined within the picosecond data at excess energies greater than 462 cm^{-1} and is of the order of 1 ns. The 47 cm^{-1} and 290 cm^{-1} traces are fit with a single decay of about 4 ns. It cannot be determined on the picosecond timescale whether or not this 4 ns decay fills a secondary state, so we employ nanosecond timescale experiments to obtain more information.

The nanosecond lasers are too slow to measure dynamics that occur on shorter timescales, but can be used to fit longer lived pathways. Upon inspection of the nanosecond pump-probe traces (Figure 6**)**, it is evident that a long lived dark state is populated which returns to the ground state on the order of a few microseconds (τ_3). This result suggests the secondary state in the picosecond experiments that decays within single nanoseconds (τ_2) may be a "doorway" state (DS_2) that feeds a long lived "dark" state (DS_1) which is observed in the nanosecond experiment as having the microsecond lifetime τ_3. The nanosecond pump-probe data were fit with primary

and secondary decays, however, in this case the primary decay is from DS_2 which decays with time constant τ_2 into DS_1 with a lifetime τ_3. The 1 ns (τ_2) decay from DS_2 for peaks 679 cm^{-1} and 904 cm^{-1} is too fast to be measured by the nanosecond pump-probe, but an additional primary decay of ~20 ns was required to fit the 679 cm^{-1} and 904 cm^{-1} traces, denoted τ_{2b}, implying a double exponential decay to DS_1 at these excess energy levels. The nanosecond (τ_1) component for 47 cm^{-1} and 290 cm^{-1} was fit in both the picosecond and nanosecond traces to within 4% and we report the average value. We assume that for these two excitations the nanosecond decay is from the bright state, not a dark state.

9-enol Guanine

We performed pump-probe experiments on 9e guanine to compare dynamics with 9e-6TG. The excitation wavelength of 32,873 cm^{-1} selects the origin of this tautomer, based on previous results.[41, 59] Measurements in the picosecond range show a flat line, indicating that there are no fast dynamics to capture at that timescale. Supplemental Figure 1 shows the nanosecond trace of the 9e guanine origin revealing two ns lifetime components. One decay path with a 40 ns lifetime feeds a long lived dark state while the other goes directly to the ground state with a 13 ns lifetime. Tautomer selective molecular beam LIF experiments performed by Chin et al. found a 12 ± 2 ns fluorescence lifetime when 9e guanine was excited at its origin.[40] A 50 ns collection window was used in that work and a two-state mixing model $\{S_2,S_1) \rightarrow S_0$ was given to support the broad dispersed fluorescence spectrum. Without a picosecond component to experimentally confirm the $S_2 \rightarrow S_1$ hypothesis we interpret the faster 13 ns decay as fluorescence from the optically bright state. The slower 40 ns decay then feeds a dark state with no fluorescent signature, which could be a $^1n\pi^*$ or a triplet state. In support of the Chin branching model, it is possible that if S_2 is the initially excited state, vibronic equilibration between S_2 and S_1 occurs on a sub-picosecond timescale leading to fluorescence at rates that are equal or undistinguishable by these experiments. Since in solution guanine exists predominantly in the keto form this is to our knowledge the first observation of such a long lived dark state in enol guanine. If the 13 and 40 ns decays are the only two excited state processes, then the fluorescence quantum yield is about 75%.

Computational Results

The CCSD energy calculations for the excited states indicate that excitation is to the S_1 state based on oscillator strengths for 9e, 7e 6-TG, and 9e guanine (Supplementary Table 1). This conclusion suggests ruling out the option that τ_1 could be the decay of S_2 to S_1 and instead suggests that τ_1 describes ISC, populating a DS_2 of triplet state character. Such fast ISC can be further explained when combined with information from CASSCF calculations. The 10 SHARC trajectories produce one conical intersection (CI) for S_1/S_0 internal conversion and two relevant intersystem crossing geometries for El-Sayed allowed $S_1(\pi\pi^*)/T_3(n\pi^*)$ and forbidden $S_1(\pi\pi^*)/T_2(\pi\pi^*)$ crossings. The CI involves the loss of the SH hydrogen, where the S_1/T_3 ISC path involves a distortion of the heterocycle (ISC_{dist}), and the S_1/T_2 path corresponds to an out of plane rotation of the thiol group (ISC_{oop}) (Figure 7**)**. These are preliminary simulations only for the 9e tautomer, consistent with the experimental structural findings described above. We cannot

exclude the presence of a second rotamer and of a 7e tautomer so a follow-up comprehensive computational treatment at a higher level will need to also consider those tautomers.

Figure 8a-c shows LIIC plots constructed by stepping the internal coordinates from the FC geometry to the CI/ISC of interest. The path to the CI (Figure 8a) has no barrier, and can be accessed from all excess energies in the FC region. The LIIC for ISC_{oop} (Figure 8b) results in a barrierless path for a S_1/T_2 crossing being located well below the FC region. The transition is forbidden, but with larger spin orbit coupling due to the sulfur, could be much faster than without it. It also appears that this path results in the singlet and second triplet state being in close proximity, in fact crossing multiple times between the 5^{th} and 8^{th} pathway intervals, which could increase the probability of making the transition at the ISC_{oop} geometry. The ISC_{dist} pathway (Figure 8c) involves a crossing seam which starts around 0 cm^{-1} of excess energy, and extends to nearly 9,000 cm^{-1}. Since this ISC transition is El-Sayed allowed, ultrafast ISC is expected if the crossing is reached which may not be the case considering IVR in the excited state will distribute energy across all modes rather than in the direction of the LIIC.

Like in the LIIC ISC pathway to T_2 (Figure 8b) there are additional crossing points on the potential surface for ISC to T_3 possibly indicating that additional geometries exist for ISC which over the timescale of the SHARC calculations were not populated. It could also be that a greater number of trajectories would yield additional crossing geometries along with statistically significant likelihoods for each. These energy crossings within the LIIC curves may also be artifacts of the level of theory and of plotting a linear interpolation as opposed to a minimum energy pathway.

4. Discussion

Intersystem crossing is typically a slow process due to the required spin flip, but may be ultrafast when spin orbit coupling is large. Increases in spin orbit coupling may happen in various ways, such as a change in symmetry or through the heavy atom effect.[25, 46] We measured excited state lifetimes with increasing excess energy to learn more about possible decay pathways in 6-TG. We performed SHARC simulations initiating in the S_2 state so that internal conversion to S_1 produces a hot excited state. By performing simulations in this manner, we can find crossing geometries that have an activation barrier, which may be accessed with larger amounts of internal energy.

Based on the assumption that excitation of 9e-6TG results in population of S_1, the initial decay can go to either the ground state (IC) or a triplet state (ISC). The picosecond pump-probe data indicates initial decay to a doorway DS_2 state, suggesting that fast ISC is occurring. We do not observe direct decay to the ground state on the timescales of our experiments, suggesting the absence of IC. This result is interesting because Figure 8a shows a conical intersection located below the Frank-Condon region. It may be that IC occurs quicker than the picosecond laser pulse widths, obscuring this pathway in our experiments. Without certainty that all processes are observed we cannot derive quantum yields from the rates, but we can compare observed (τ_1^{-1}) and (τ_2^{-1}) rates with the 40 ns decay to the long lived dark state of 9e guanine. Here it seems that the sulfur←oxo substitution quenches the 75% fluorescence decay seen in 9H-G_e in favor of total population redistribution to the long-lived excited state in 9e-6TG. Additionally, this long-lived

dark state is directly populated in the guanine case but proceeds through a doorway state in 6-TG. This comparison is generalized in Figure 9 cases (a) and (c) for the 6-TG and guanine models respectively.

Figure 9 (a,b) summarizes a tentative interpretation of the pump-probe observations of 9e-6TG with two cases. Case (a) corresponds to excitation at 0, 462, 679, and 904 cm^{-1} and case (b) corresponds to excitation at 47 and 290 cm^{-1}. A possible explanation involving two different relaxation mechanisms is that the excess energy traces included excitations of multiple thiol forms that went unresolved by mode II IR hole burning measurements. Neither the 7e tautomer nor a rotational isomer, about the thiol dihedral coordinate, can be excluded. Alternatively, there may be some vibronic selection criteria which strongly mediate relaxation to either case for 9e-6TG. In these models the first decay τ_1 represents total population transfer from the bright state S_n to DS_2 for (a) and to DS for (b). DS_2 provides a pathway to DS_1 by two measurable decay rates, τ_2^{-1} and τ_{2b}^{-1}. The latter rate, τ_{2b}^{-1}, has an empirical vibronic energy barrier of +679 cm^{-1} (upper limit). Case (a) then decays at τ_3^{-1} from DS_1 to below the ionization potential of our probe laser, into what is likely the ground state of 6-TG. In case (b) τ_1 feeds directly into the long-lived DS, which then decays at τ_3^{-1} on a microsecond timescale. The microsecond relaxation time may lend credence to the identity of DS_1 and DS as triplet states.

A thorough theoretical model is needed to correlate the pump-probe dynamics with specific electronic state identities and trajectory mechanisms. Our preliminary LIIC results provide trends of IC and ISC from the 9e-6TG FC geometry, at the CASSCF level, as initial insight. Figure 8b supports the notion that the S_1/T_2 crossing occurs below the Frank-Condon geometry. Figure 8c shows an S_1/T_3 crossing well above the Frank-Condon geometry with S_1 and T_2 intersecting along this path as well. This suggests that ISC, likened to τ_1, is occurring quickly to T_2 at the energies probed here, and that with even more energy (around +679 cm^{-1}), T_3 may be accessed which would provide access to an El-Sayed allowed transition. In this case T_3/T_2 conversion would be rapid and could yield the τ_2^{-1} and τ_{2b}^{-1} rates seen at higher energies.

5. Conclusion

When comparing the dynamics of the thiol system studied here with the aqueous phase femtosecond study of the thione-nucleoside by Reichardt et al.[43] interpreted by Martínez-Fernández et al.,[30, 44] the rates for ISC are 300-1000 times lower for the thiol. Reichardt also saw internal conversion occurring on the tens of picoseconds timescale, which we do not see in the thiol in the gas phase. In addition to the lack of tautomer selectivity, aqueous phase experiments can produce different results because the solvent affects excited state dynamics by hydrogen bonding and structural changes. Possible ISC lifetimes for 9k and 7k tautomers of 6-thioguanine in the gas phase for comparison are unknown. We demonstrated the effect on ISC of replacing the oxygen in guanine with a sulfur by comparing the pump-probe results of 9e 6-TG with those of 9e guanine. The guanine data correspond to fluorescence lifetimes and a lower decay, possibly ISC, of 13 ns and 40 ns, respectively. At the origin the rate (τ_1^{-1}) for filling DS_2 in 9e 6-TG is 80 times greater than the decay to the long lived dark state in 9e guanine. Lastly, the presence of an intermediary state (DS_2) is not seen when probing 9e guanine. Higher level computations are needed for a more complete interpretation of the experimental results.

Supporting Information

Singlet and triplet excited state analysis at CCSD/6-31+G(2d,p) for ground state and EOM-CCSD/6-31+G(2d,p) for excited states, nanosecond pump probe trace of 9-enol guanine at its origin.

Acknowledgments

This work was supported by National Aeronautics and Space Administration Grant NNX12AG77G and by the National Science Foundation under CHE-1301305. We acknowledge support from the Center for Scientific Computing from the CNSI, MRL: an NSF MRSEC (DMR-1121053) and NSF CNS-0960316.

References

1. He, Y. G.; Wu, C. Y.; Kong, W. Decay Pathways of Thymine and Methyl-Substituted Uracil and Thymine in the Gas Phase. *J. Phys. Chem. A* **2003,** *107*, 5145-5148.
2. Gengeliczki, Z.; Callahan, M. P.; Svadlenak, N.; Pongor, C. I.; Sztaray, B.; Meerts, L.; Nachtigallova, D.; Hobza, P.; Barbatti, M.; Lischka, H.; de Vries, M. S. Effect of Substituents on the Excited-State Dynamics of the Modified DNA Bases 2,4-Diaminopyrimidine and 2,6-Diaminopurine. *Phys. Chem. Chem. Phys.* **2010,** *12*, 5375-5388.
3. Etinski, M.; Fleig, T.; Marian, C. M. Intersystem Crossing and Characterization of Dark States in the Pyrimidine Nucleobases Uracil, Thymine, and 1-Methylthymine. *J. Phys. Chem. A* **2009,** *113*, 11809-11816.
4. Trachsel, M. A.; Lobsiger, S.; Schar, T.; Leutwyler, S. Low-Lying Excited States and Nonradiative Processes of 9-Methyl-2-Aminopurine. *J. Chem. Phys.* **2014,** *140*, 044331.
5. Kunitski, M.; Nosenko, Y.; Brutschy, B. On the Nature of the Long-Lived "Dark" State of Isolated 1-Methylthymine. *Chemphyschem* **2011,** *12*, 2024-2030.
6. Nir, E.; Kleinermanns, K.; Grace, L.; de Vries, M. S. On the Photochemistry of Purine Nucleobases. *J. Phys. Chem. A* **2001,** *105*, 5106-5110.
7. Malone, R. J.; Miller, A. M.; Kohler, B. Singlet Excited-State Lifetimes of Cytosine Derivatives Measured by Femtosecond Transient Absorption. *Photochem. Photobiol.* **2003,** *77*, 158-164.
8. Trachsel, M. A.; Wiedmer, T.; Blaser, S.; Frey, H. M.; Li, Q.; Ruiz-Barragan, S.; Blancafort, L.; Leutwyler, S. The Excited-State Structure, Vibrations, Lifetimes, and Nonradiative Dynamics of Jet-Cooled 1-Methylcytosine. *J. Chem. Phys.* **2016,** *145*, 134307.
9. Brister, M. M.; Crespo-Hernandez, C. E. Direct Observation of Triplet-State Population Dynamics in the Rna Uracil Derivative 1-Cyclohexyluracil. *J. Phys. Chem. Lett.* **2015,** *6*, 4404-4409.
10. Lobsiger, S.; Frey, H. M.; Leutwyler, S. Supersonic Jet Uv Spectrum and Nonradiative Processes of the Thymine Analogue 5-Methyl-2-Hydroxypyrimidine. *Phys. Chem. Chem. Phys.* **2010,** *12*, 5032-5040.
11. Nachtigallova, D.; Lischka, H.; Szymczak, J. J.; Barbatti, M.; Hobza, P.; Gengeliczki, Z.; Pino, G.; Callahan, M. P.; de Vries, M. S. The Effect of C5 Substitution on the Photochemistry of Uracil. *Phys. Chem. Chem. Phys.* **2010,** *12*, 4924-4933.
12. Pollum, M.; Martínez-Fernández, L.; Crespo-Hernández, C. E. Photochemistry of Nucleic Acid Bases and Their Thio- and Aza-Analogues in Solution. In *Photoinduced Phenomena in Nucleic Acids I: Nucleobases in the Gas Phase and in Solvents*, Barbatti, M.; Borin, A. C.; Ullrich, S., Eds. Springer International Publishing: Cham, **2015**, pp 245-327.

13. Tomic, K.; Tatchen, J.; Marian, C. M. Quantum Chemical Investigation of the Electronic Spectra of the Keto, Enol, and Keto-Imine Tautomers of Cytosine. *J. Phys. Chem. A* **2005,** *109*, 8410-8418.
14. Plutzer, C.; Kleinermanns, K. Tautomers and Electronic States of Jet-Cooled Adenine Investigated by Double Resonance Spectroscopy. *Phys. Chem. Chem. Phys.* **2002,** *4*, 4877-4882.
15. Marian, C. M. The Guanine Tautomer Puzzle: Quantum Chemical Investigation of Ground and Excited States. *J. Phys. Chem. A* **2007,** *111*, 1545-1553.
16. Canuel, C.; Mons, M.; Piuzzi, F.; Tardivel, B.; Dimicoli, I.; Elhanine, M. Excited States Dynamics of DNA and Rna Bases: Characterization of a Stepwise Deactivation Pathway in the Gas Phase. *J. Chem. Phys.* **2005,** *122*, 074316.
17. Nachtigallova, D.; Hobza, P.; Spirko, V. Assigning the Nh Stretches of the Guanine Tautomers Using Adiabatic Separation: Ccsd(T) Benchmark Calculations. *J. Phys. Chem. A* **2008,** *112*, 1854-1856.
18. Seefeld, K.; Brause, R.; Haber, T.; Kleinermanns, K. Imino Tautomers of Gas-Phase Guanine from Mid-Infrared Laser Spectroscopy. *J. Phys. Chem. A* **2007,** *111*, 6217-6221.
19. Mons, M.; Piuzzi, F.; Dimicoli, I.; Gorb, L.; Leszczynski, J. Near-Uv Resonant Two-Photon Ionization Spectroscopy of Gas Phase Guanine: Evidence for the Observation of Three Rare Tautomers. *J. Phys. Chem. A* **2006,** *110*, 10921-10924.
20. Cerny, J.; Spirko, V.; Mons, M.; Hobza, P.; Nachtigallova, D. Theoretical Study of the Ground and Excited States of 7-Methyl Guanine and 9-Methyl Guanine: Comparison with Experiment. *Phys. Chem. Chem. Phys.* **2006,** *8*, 3059-3065.
21. Hare, P. M.; Crespo-Hernandez, C. E.; Kohler, B. Internal Conversion to the Electronic Ground State Occurs Via Two Distinct Pathways for Pyrimidine Bases in Aqueous Solution. *Proc. Natl. Acad. Sci. USA* **2007,** *104*, 435-440.
22. Serrano-Andres, L.; Merchan, M. Are the Five Natural DNA/Rna Base Monomers a Good Choice from Natural Selection? A Photochemical Perspective. *J. Photochem. Photobio., C* **2009,** *10*, 21-32.
23. Yamazaki, S.; Domcke, W.; Sobolewski, A. L. Nonradiative Decay Mechanisms of the Biologically Relevant Tautomer of Guanine. *J. Phys. Chem. A* **2008,** *112*, 11965-11968.
24. Mons, M.; Dimicoli, I.; Piuzzi, F. Isolated Guanine: Tautomerism, Spectroscopy and Excited State Dynamics. In *Radiation Induced Molecular Phenomena in Nucleic Acids: A Comprehensive Theoretical and Experimental Analysis*, Shukla, M. K.; Leszczynski, J., Eds. Springer Netherlands: Dordrecht, **2008**, pp 343-367.
25. Koziar, J. C.; Cowan, D. O. Photochemical Heavy-Atom Effects. *Acc. Chem. Res.* **1978,** *11*, 334-341.
26. Rubin, Y. V.; Blagoi, Y. P.; Bokovoy, V. A. 6-Thioguanine Luminescence Probe to Study DNA and Low-Molecular-Weight Systems. *J. Fluoresc.* **1995,** *5*, 263-272.
27. Ashwood, B.; Jockusch, S.; Crespo-Hernandez, C. E. Excited-State Dynamics of the Thiopurine Prodrug 6-Thioguanine: Can N9-Glycosylation Affect Its Phototoxic Activity? *Molecules* **2017,** *22*.
28. Stewart, M. J.; Leszczynski, J.; Rubin, Y. V.; Blagoi, Y. P. Tautomerism of Thioguanine: From Gas Phase to DNA. *J. Phys. Chem. A* **1997,** *101*, 4753-4760.
29. Yu, H.; Sanchez-Rodriguez, J. A.; Pollum, M.; Crespo-Hernandez, C. E.; Mai, S.; Marquetand, P.; Gonzalez, L.; Ullrich, S. Internal Conversion and Intersystem Crossing Pathways in Uv Excited, Isolated Uracils and Their Implications in Prebiotic Chemistry. *Phys. Chem. Chem. Phys.* **2016,** *18*, 20168-20176.
30. Martinez-Fernandez, L.; Corral, I.; Granucci, G.; Persico, M. Competing Ultrafast Intersystem Crossing and Internal Conversion: A Time Resolved Picture for the Deactivation of 6-Thioguanine. *Chem. Sci.* **2014,** *5*, 1336-1347.
31. Kang, H.; Lee, K. T.; Jung, B.; Ko, Y. J.; Kim, S. K. Intrinsic Lifetimes of the Excited State of DNA and Rna Bases. *J. Am. Chem. Soc.* **2002,** *124*, 12958-12959.
32. Karran, P.; Attard, N. Thiopurines in Current Medical Practice: Molecular Mechanisms and Contributions to Therapy-Related Cancer. *Nat. Rev. Cancer* **2008,** *8*, 24-36.

33. Euvrard , S.; Kanitakis , J.; Claudy , A. Skin Cancers after Organ Transplantation. *N. Engl. J. Med.* **2003,** *348*, 1681-1691.
34. Kaplan, H. S.; Smith, K. C.; Tomlin, P. Radiosensitization of E. Coli by Purine and Pyrimidine Analogues Incorporated in Deoxyribonucleic Acid. *Nature* **1961,** *190*, 794-796.
35. Cuffari, C.; Li, D. Y.; Mahoney, J.; Barnes, Y.; Bayless, T. M. Peripheral Blood Mononuclear Cell DNA 6-Thioguanine Metabolite Levels Correlate with Decreased Interferon-Gamma Production in Patients with Crohn's Disease on Aza Therapy. *Dig. Dis. Sci.* **2004,** *49*, 133-137.
36. Zhang, X. H.; Jeffs, G.; Ren, X. L.; O'Donovan, P.; Montaner, B.; Perrett, C. M.; Karran, P.; Xu, Y. Z. Novel DNA Lesions Generated by the Interaction between Therapeutic Thiopurines and Uva Light. *DNA Repair* **2007,** *6*, 344-354.
37. O'Donovan, P.; Perrett, C. M.; Zhang, X.; Montaner, B.; Xu, Y.-Z.; Harwood, C. A.; McGregor, J. M.; Walker, S. L.; Hanaoka, F.; Karran, P. Azathioprine and Uva Light Generate Mutagenic Oxidative DNA Damage. *Science* **2005,** *309*, 1871-1874.
38. Montaner, B.; O'Donovan, P.; Reelfs, O.; Perrett, C. M.; Zhang, X.; Xu, Y. Z.; Ren, X.; Macpherson, P.; Frith, D.; Karran, P. Reactive Oxygen-Mediated Damage to a Human DNA Replication and Repair Protein. *EMBO Rep* **2007,** *8*, 1074-1079.
39. Attard, N. R.; Karran, P. Uva Photosensitization of Thiopurines and Skin Cancer in Organ Transplant Recipients. *Photochem. Photobiol. Sci.* **2012,** *11*, 62-68.
40. Chin, W.; Mons, M.; Dimicoli, I.; Piuzzi, F.; Tardivel, B.; Elhanine, M. Tautomer Contributions to the near Uv Spectrum of Guanine: Towards a Refined Picture for the Spectroscopy of Purine Molecules. *Euro. Phys. J. D.* **2002,** *20*, 347-355.
41. Nir, E.; Janzen, C.; Imhof, P.; Kleinermanns, K.; de Vries, M. S. Guanine Tautomerism Revealed by Uv-Uv and Ir-Uv Hole Burning Spectroscopy. *J. Chem. Phys.* **2001,** *115*, 4604-4611.
42. Choi, M. Y.; Miller, R. E. Four Tautomers of Isolated Guanine from Infrared Laser Spectroscopy in Helium Nanodroplets. *J. Am. Chem. Soc.* **2006,** *128*, 7320-7328.
43. Reichardt, C.; Guo, C.; Crespo-Hernandez, C. E. Excited-State Dynamics in 6-Thioguanosine from the Femtosecond to Microsecond Time Scale. *J. Phys. Chem. B* **2011,** *115*, 3263-3270.
44. Martinez-Fernandez, L.; Gonzalez, L.; Corral, I. An Ab Initio Mechanism for Efficient Population of Triplet States in Cytotoxic Sulfur Substituted DNA Bases: The Case of 6-Thioguanine. *Chem. Commun.* **2012,** *48*, 2134-2136.
45. Mai, S.; Pollum, M.; Martinez-Fernandez, L.; Dunn, N.; Marquetand, P.; Corral, I.; Crespo-Hernandez, C. E.; Gonzalez, L. The Origin of Efficient Triplet State Population in Sulfur-Substituted Nucleobases. *Nat. Commun.* **2016,** *7*, 13077.
46. El - Sayed, M. A. Spin—Orbit Coupling and the Radiationless Processes in Nitrogen Heterocyclics. *J. Chem. Phys.* **1963,** *38*, 2834-2838.
47. Meijer, G.; Devries, M. S.; Hunziker, H. E.; Wendt, H. R. Laser Desorption Jet-Cooling of Organic-Molecules - Cooling Characteristics and Detection Sensitivity. *Appl. Phys. B.* **1990,** *51*, 395-403.
48. Irimia, D.; Dobrikov, D.; Kortekaas, R.; Voet, H.; van den Ende, D. A.; Groen, W. A.; Janssen, M. H. A Short Pulse (7 Micros Fwhm) and High Repetition Rate (Dc-5 Khz) Cantilever Piezovalve for Pulsed Atomic and Molecular Beams. *Rev. Sci. Instrum.* **2009,** *80*, 113303.
49. Lipert, R. J.; Bermudez, G.; Colson, S. D. Pathways of S1 Decay in Phenol, Indoles, and Water Complexes of Phenol and Indole in a Free Jet Expansion. *J. Phys. Chem.* **1988,** *92*, 3801-3805.
50. Spesyvtsev, R. Experimental Investigation of Ultrafast Internal Conversion in Aniline and 1,4-Diazabicyclo[2.2.2]Octane (Dabco). UCL (University College London), **2013**.
51. Wolfram Research, I. *Mathematica*, 10.0; Wolfram Research, Inc.: Champaign, Illinois, **2014**.
52. Frisch, M. J.; Trucks, G. W.; Schlegel, H. B.; Scuseria, G. E.; Robb, M. A.; Cheeseman, J. R.; Scalmani, G.; Barone, V.; Mennucci, B.; Petersson, G. A.; et al. Gaussian 09, Revision B.01. Wallingford CT, **2009**.

53. Mai, S. R., M.; Ruckenbauer, M.; Oppel, M.; Marquetand, P.; González, L. *Sharc: Surface Hopping Including Arbitrary Couplings – Program Package for Non-Adiabatic Dynamics*, sharc-md.org, **2014**.
54. Richter, M.; Marquetand, P.; González-Vázquez, J.; Sola, I.; González, L. Sharc: Ab Initio Molecular Dynamics with Surface Hopping in the Adiabatic Representation Including Arbitrary Couplings. *J. Chem. Theory Comput.* **2011,** *7*, 1253-1258.
55. Werner, H.-J.; Knowles, P. J.; Knizia, G.; Manby, F. R.; Schütz, M. Molpro: A General-Purpose Quantum Chemistry Program Package. *Wiley Interdisciplinary Reviews: Computational Molecular Science* **2012,** *2*, 242-253.
56. Crespo-Hernandez, C. E.; Martinez-Fernandez, L.; Rauer, C.; Reichardt, C.; Mai, S.; Pollum, M.; Marquetand, P.; Gonzalez, L.; Corral, I. Electronic and Structural Elements That Regulate the Excited-State Dynamics in Purine Nucleobase Derivatives. *J. Am. Chem. Soc.* **2015,** *137*, 4368-4381.
57. Kasende, O. E. Infrared Spectra of 6-Thioguanine Tautomers. An Experimental and Theoretical Approach. *Spectrochim. Acta. Mol. Biomol. Spectrosc.* **2002,** *58*, 1793-1808.
58. Plutzer, C.; Nir, E.; de Vries, M. S.; Kleinermanns, K. Ir-Uv Double-Resonance Spectroscopy of the Nucleobase Adenine. *Phys. Chem. Chem. Phys.* **2001,** *3*, 5466-5469.
59. Nir, E.; Grace, L.; Brauer, B.; de Vries, M. S. Rempi Spectroscopy of Jet-Cooled Guanine. *J. Am. Chem. Soc.* **1999,** *121*, 4896-4897.

Tables

Fitting Parameters for 6-Thioguanine

Excess Energy [cm^{-1}]	τ_1, ps	τ_2, ns	τ_{2b}, ns	τ_3, ns
0	481 [a]	6.1 [b]		2025 [b]
47	3920 [ab]			3033 [b]
290	4330 [ab]			2000 [b]
462	577 [a]	5.7 [b]		2590 [b]
679	87 [a]	0.9 [a]	24 [b]	878 [b]
904	168 [a]	1.1 [a]	21.5 [b]	462 [b]

Table 1. Summary of fitting parameters where [a] denotes a value from picosecond fit and [b] denotes a value from a nanosecond fit.

Figures

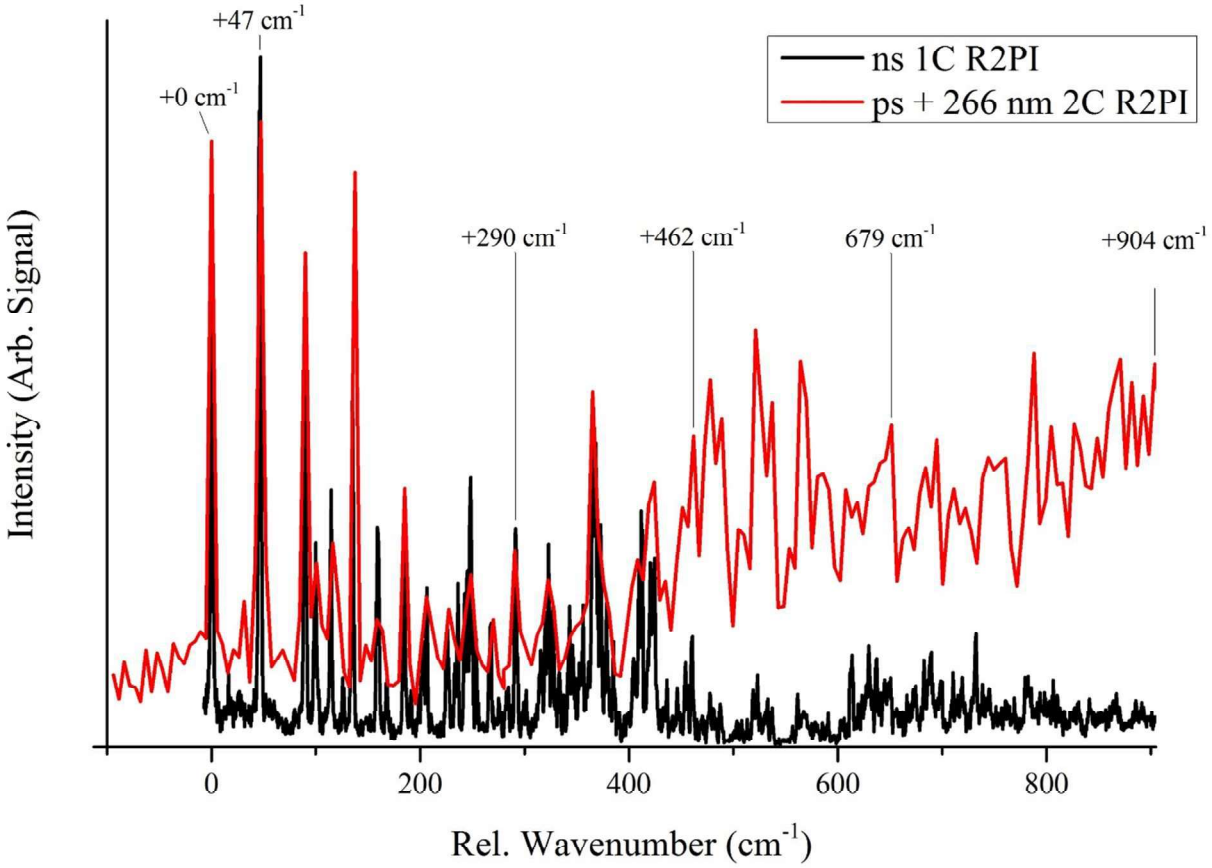

Figure 1. One-color resonant two-photon nanosecond ionization spectrum of jet-cooled 6-thioguanine is shown in black and two-color resonant two-photon picosecond ionization spectrum of jet-cooled 6-thioguanine is shown in red. The wavenumber scale is relative to the 0_0^0 band at 32,343 cm^{-1} and annotations mark where pump-probe was performed. Both spectra have been normalized at +0 cm^{-1}.

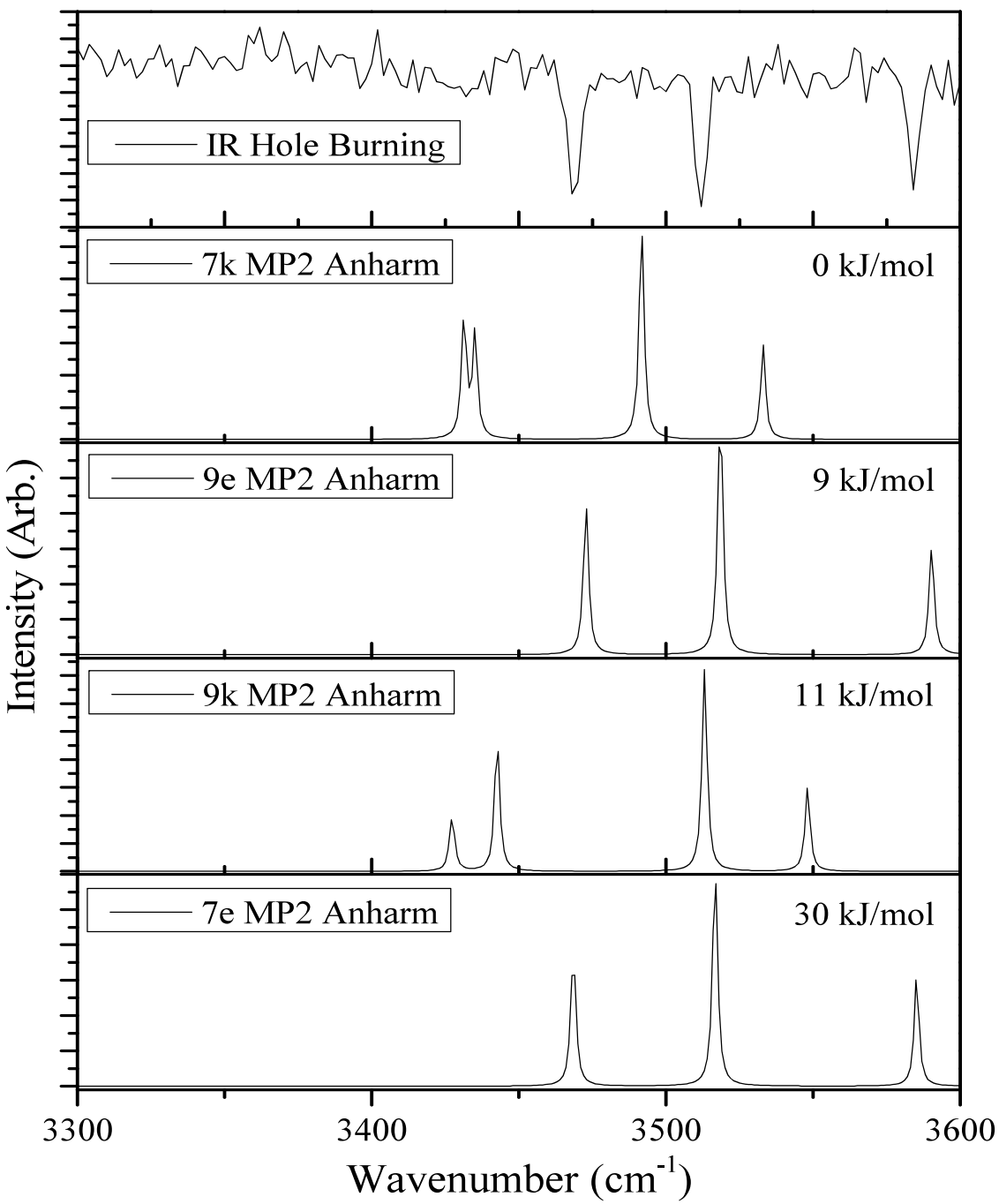

Figure 2. Experimental IR hole burning spectrum in mode I (*top*) and theoretical IR bands calculated at the anharmonic MP2/6-31+G(2d,p) level. Energies shown calculated at CCSD/6-31+G(2d,p).

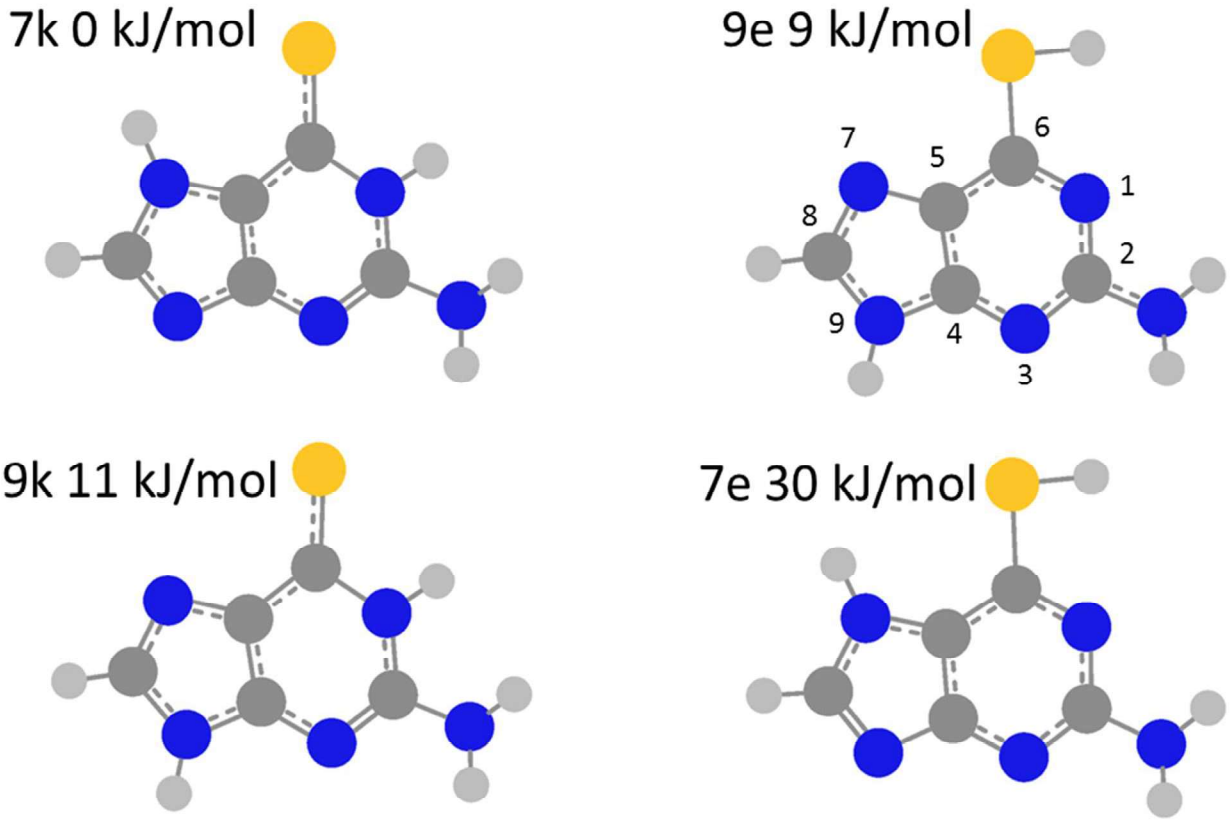

Figure 3. Ground state (Frank-Condon) structures optimized at MP2/6-31+G(2d,p). The atom numbering is shown on the 9e tautomer. Energies shown calculated at CCSD/6-31+G(2d,p).

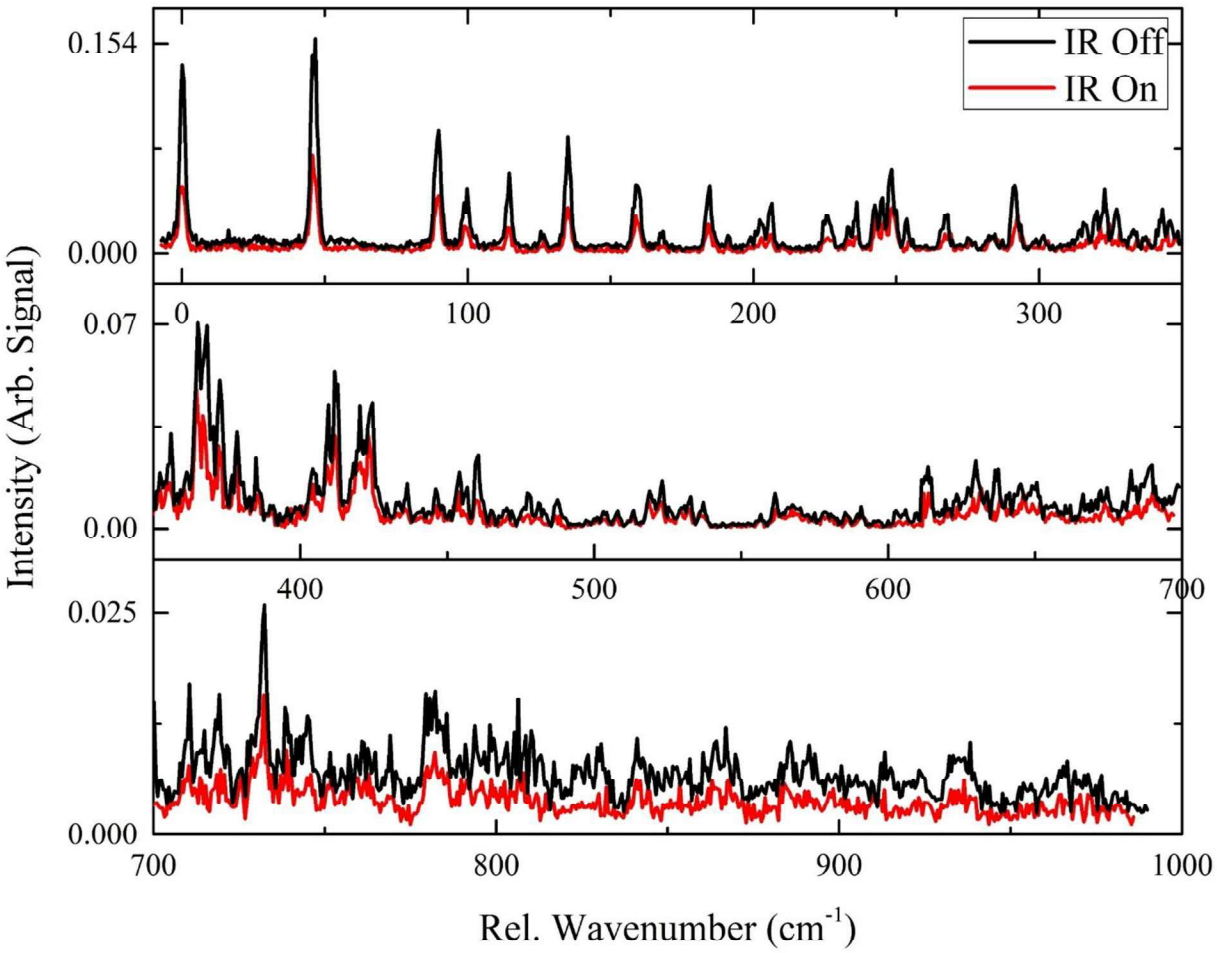

Figure 4. IR laser set to 3,584 cm^{-1} 200 ns prior to scanning UV. Decrease in signal indicates shared IR resonance with the origin transition.

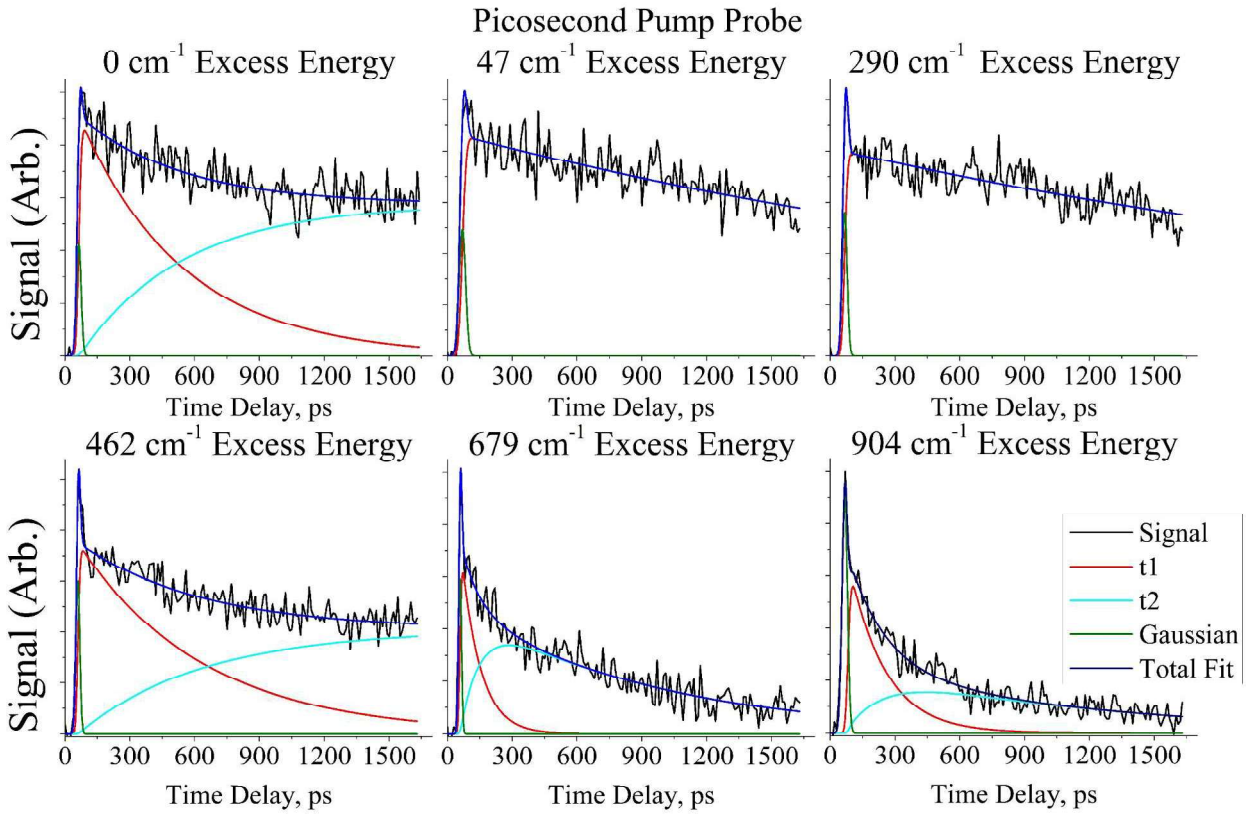

Figure 5: Picosecond pump-probe traces with fitting for 0, 47, 290, 462, 679, and 904 cm^{-1}. Fitting parameters are marked as [a] in Table 1.

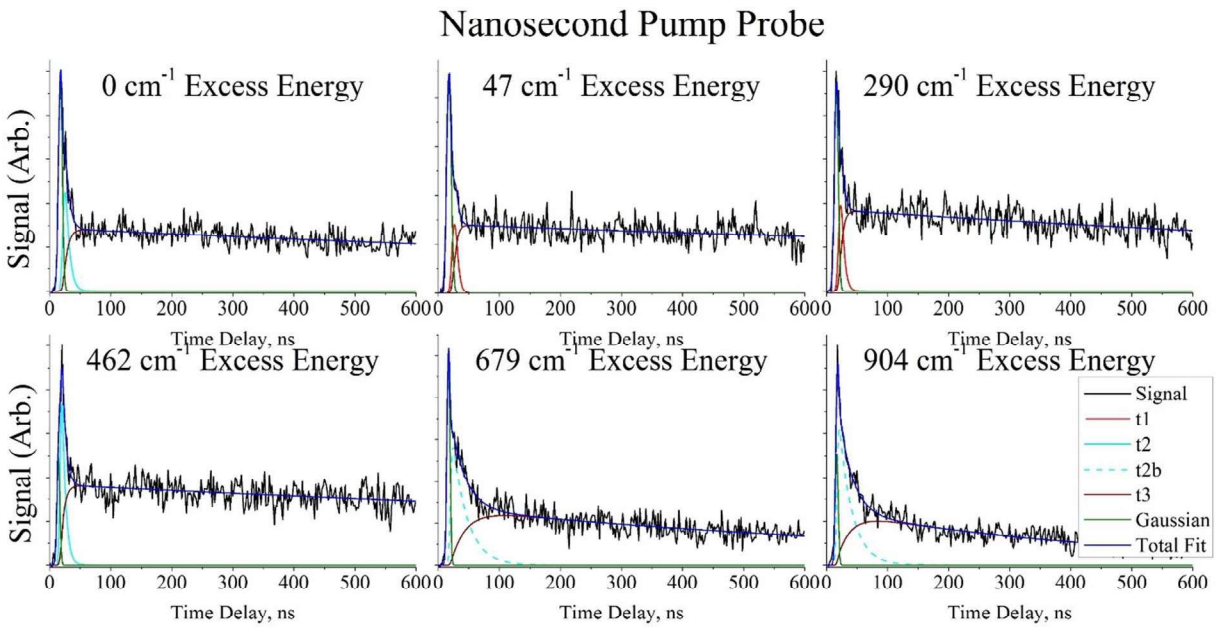

Figure 6. Nanosecond pump-probe traces with fitting for 0, 47, 290, 462, 679, and 904 cm^{-1}. Fitting parameters are marked as [b] in Table 1.

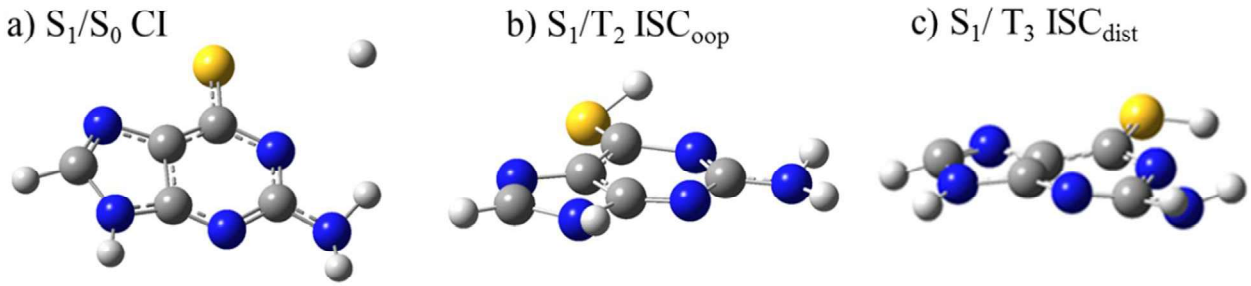

Figure 7. Structures are geometries leading to hops in the SHARC simulation. All structures are calculated at SA-CASSCF(10,10)/6-31G(d) level.

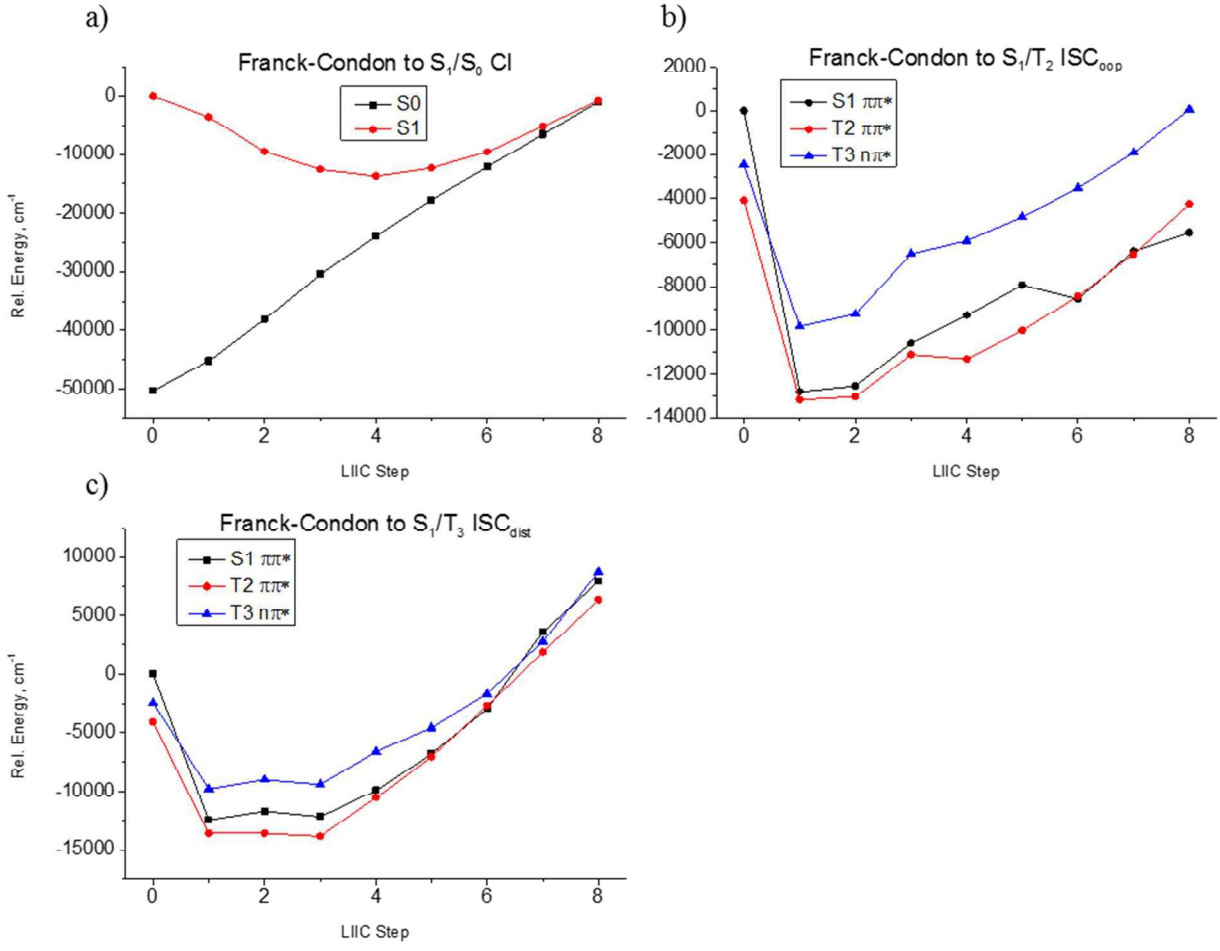

Figure 8. LIIC curves using SA-CASSCF(10,10)/6-31G* from the Frank-Condon geometry to the a) conical intersection, b) ISC path to ISC_{oop}, and c) ISC path to ISC_{dist}

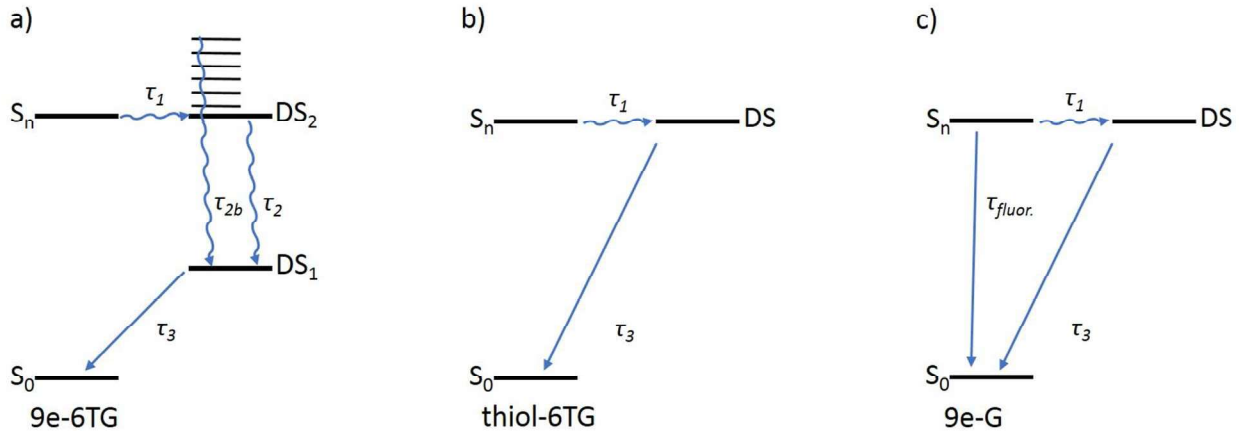

Figure 9. Proposed decay pathways where a) corresponds to traces 0, 462, 679, and 904 cm^{-1} and b) corresponds to traces 47 and 290 cm^{-1} of 6-TG and c) corresponds to the 0 cm^{-1} trace of 9e guanine. S_n is the assumed to be the optically bright state probed by picosecond resolution. DS_2, and S_n of (b) and (c), are assumed to be the initial decay states probed by nanosecond resolution. τ_{2b} has an activation barrier of +679 cm^{-1} (upper limit).

TOC Graphic

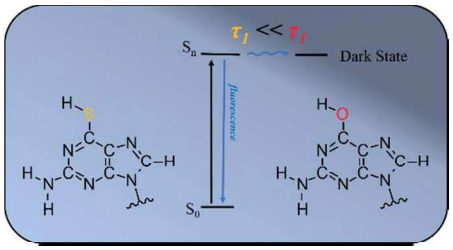
$\tau_1 \ll \tau_1$
S_n
Dark State
fluorescence
S_0
H
S
N
C
N
C–H
H
N
H
N
H
O
N
C
N
C–H
H
N
H